This is a shortened version of the manuscript under review in journal Geophysical & Astrophysical Fluid Dynamics

New method for a three-dimensional turbulence detection as a deviation from local hydrostatic balance

Petr Šácha[1,2] and Petr Pišoft[1]

[1]*Department of Atmospheric Physics, Faculty of Mathematics and Physics, Charles University, Prague, Czech Republic*

[2]*Institute of Meteorology, University of Natural Resources and Life Sciences, Vienna (BOKU), Vienna, Austria*

petr.sacha@boku.ac.at

Introduction

In the presented study we propose a new method for detection of three-dimensional turbulence applicable to high vertical-resolution radiosonde data (HVRRD), or any other simultaneous measurements of vertical profiles of the temperature, pressure and humidity (for application in the troposphere). Our motivation for proposing a new method for turbulence detection is connected with the most familiar effect of the clear-air turbulence (CAT) - variations of the vertical lift (e.g. causing the bumpiness of the airplane). Three-dimensional atmospheric turbulence is characterised by irregular fluctuations in all velocity components in situations, when the inertial forces dominate. Thus, from its definition, the hydrostatic balance does not hold in turbulent layers. HVRRD allow to compute the deviation from local hydrostatic balance directly, from the knowledge of pressure, temperature and RH profiles and using the vertical component of Euler equations, which relates the deviation directly to the total derivative of vertical

momentum. To tackle the presence of noise in HVRRD, we further integrate the equation vertically and the deviations than get an illustrative form of a difference of the observed and hydrostatically derived pressure. The methodology is demonstrated on selected observational events. For comparison, the traditional methods for turbulence identification are computed. In the discussion, future work and relation with theoretical characteristics of turbulence is outlined.

Methodology

Method

Considering high Rossby and Reynolds number regimes, the Navier-Stokes equations reduce to Eulerian equations. Assuming that in the free atmosphere there are no external forces in the vertical direction, we start by writing the vertical component of the compressible Euler equations:

$$\frac{d\rho w}{dt} = -\frac{\partial p}{\partial z} - \rho g, \tag{1}$$

where ρ is the density and p the pressure of air, w is the vertical velocity component and g the gravitational acceleration (generally a function of altitude, latitude and longitude). The zeroth right hand side is a typical signature of hydrostatic balance for incompressible fluids and equation (1) relates the hydrostatic balance deviations (HBDs) to a total derivative of the vertical momentum.

An illustrative and useful form of the equation can be obtained after a small manipulation of eq. (1). Integrating the equation vertically at arbitrarily small domains, we get deviations of the observed pressure from hydrostatically derived pressure. Instead of integrating vertically across the whole profile and initializing the computation at the upper boundary of the analysis (common procedure for hydrostatic pressure), we select a finite width of the domain of integration (h). Therefore, also the level of initialization (z_{i+h}) differs for each level (z_i). The hydrostatic procedure is initialized from the observed pressure at the level z_{i+h}. This can be written as,

$$p_{hydr}(z_i) = p(z_{i+h}) + \int_{z_i}^{z_{i+h}} \rho g \, dz, \tag{2}$$

where $p_{hydr}(z_i)$ is the locally-hydrostatically derived pressure at the altitude z_i and $p(z_{i+h})$ is the observed pressure at z_{i+h}. Coming back to the Euler equation, we vertically integrate eq. (1) in the vertical domain of finite width h to get:

$$\int_{z_i}^{z_{i+h}} \frac{d\rho w}{dt} dz = -\int_{z_i}^{z_{i+h}} \frac{\partial p}{\partial z} dz - \int_{z_i}^{z_{i+h}} \rho g \, dz \tag{3}$$

$$= p(z_i) - p(z_{i+h}) - \int_{z_i}^{z_{i+h}} \rho g \, dz \tag{3a}$$

$$= p(z_i) - p_{hydr}(z_i). \tag{3b}$$

Equation (3b) relates the deviation between observed and hydrostatically derived pressure (i.e. HBD) with the rate of change of vertical momentum integrated in the vertical domain.

For application of eqs. (1) and (3) to HVRRD, ρ is computed from the equation of state for ideal gas using the observed pressure, temperature (T) and RH as follows:

$$\rho = p/R_d T_v, \tag{4}$$

Where R_d is the specific gas constant for dry air (287.058 $Jkg^{-1}K^{-1}$) and T_v is the so-called virtual temperature, which is a combination of the temperature, pressure and partial water vapor pressure (e):

$$T_v = T\left(1 + \frac{0.378e}{p - 0.378e}\right). \tag{5}$$

e is a product of RH (measured) and the saturation vapor pressure, which is dependent on T and is inferred using the empirical August-Roche-Magnus formula:

$$e_s(T) = 6.1094\exp\left(\frac{17.625T}{T+0.378e}\right). \quad (6)$$

Note that the temperature has to be inserted to the formula in °C. In the stratosphere, air is dry to a high precision and the virtual temperature is practically equivalent to the original temperature. In the process of density derivation, we neglect differences of the atmospheric composition other than caused by a presence of the water vapor.

For the free atmosphere we suppose the hydrostatic balance to hold at a leading order and hence HBDs and the total derivatives of vertical momentum to be ideally zero, although there could be some nonzero background effects connected with the climatological middle atmospheric large-scale vertical motions. For the vertical scales of tens of metres and less, we expect [based on typical shapes of the energy spectrum in the free atmosphere, see Staquet and Sommeria (2002), Figure 7b] that the deviations will be dominated by the vertical turbulence. In the presence of turbulence in the profile, HBD should have a typical signature indicating an overturn - a positive deviation signalling the lower boundary and a negative deviation marking the top of the overturning region.

This pattern can be deduced from the expanded material derivative of the vertical momentum in eq. (1) and by considering a single idealized overturn resulting from the convective instability. In the case of the integral method (eq. 3), the left hand side is:

$$\int_{z_i}^{z_{i+h}} \frac{d\rho w}{dt}\,dz = \int_{z_i}^{z_{i+h}} \rho \frac{dw}{dt}\,dz + \int_{z_i}^{z_{i+h}} w \frac{d\rho}{dt}\,dz. \quad (7)$$

In addition to the proposed method, traditional turbulence diagnostics are computed for comparison. The Richardson number (Ri) characterizing the onset of instability in stratified shear flow (see e.g. Wyngaard, 2010). It is traditionally assumed that Ri values below the critical value 0.25 identify unstably stratified regions and a developed turbulence. It can be computed from HVRRD directly in its gradient form (Ri_g), as a ratio of Brunt–Väisälä frequency (N) and the square of horizontal wind shear (S^2):

$$Ri_g = {N^2}/{S^2}, \quad (8)$$

where N is computed as:

$$N = \sqrt{\frac{g}{\theta_v}\frac{\partial \theta_v}{\partial z}} \quad (9)$$

and θ_v stands for the virtual potential temperature.

The Thorpe analysis (after Thorpe, 1977) is the main diagnostic of turbulence in the atmosphere allowing to estimate parameters as eddy dissipation rate (ε) and the local overturning scale (via L_T). The idea of the method stems from conservation of the potential temperature during adiabatic processes. Under stable conditions, potential temperature profiles should increase with increasing height and negative slopes of the profiles in the free atmosphere mark the overturn regions caused by breaking gravity waves or the turbulence. We follow the traditional methodology for computation of Thorpe analysis from HVRRD as explained in detail in e.g. Clayson and Kantha (2008) and Ko et al. (2019). First, high resolution θ_v profile is computed:

$$\theta_v = T_v \left(\frac{1000}{p}\right)^{0.286} \quad (10)$$

which is then resorted into a stable monotonic profile. The vertical distance that it takes to move an idealized particle with the actual observed potential temperature to a level of

its match in the stable profile is called a Thorpe displacement, whose root mean square value over the overturning region is the L_T.

Finally, we compute a simplified version of the proposed methodology that is akin to the traditional dynamic pressure concept (Vallis, 2017). Assuming small amplitude disturbances, a hydrostatic background atmosphere and neglecting dynamical density fluctuations eq. (3a) becomes:

$$\int_{z_i}^{z_{i+h}} \bar{\rho} \frac{dw'}{dt} dz = p'(z_i) - p'(z_{i+h}), \quad (11)$$

where $\bar{\rho}$ is a background density that would correspond to the state of hydrostatical balance. The profile of pressure perturbations can be derived by some statistical form of background separation, in our case by subtracting a smoothed background profile calculated by a moving average over a chosen number of neighbouring levels. Unlike in the literature, we do not interpolate the profiles to an equally spaced vertical grid (see the Discussion section for reasoning). Therefore, for the methods based on eqs. (3b) and (11) the results are divided by h to get units [Pa/m].

For the comparison of the turbulence detection methodologies, we follow Wilson et al. (2010) to reduce the impact of measurement noise on the Thorpe analysis by removing the linear trend from short segments of temperature profile (5 points), calculating the mean of the squared differences as in Wilson et al. (2010) and subsequently computing the temperature noise variance as half the average value of these means in the entire profile. Then, we go from the bottom to the top of the temperature profile, examining successive vertical levels in the profile, and setting the temperature for the succeeding level equal to the preceding level if the difference between the two temperatures does not exceed the measurement noise. As in Kantha and Hocking (2011), these modified temperature profiles are then used for the Thorpe analysis. Similar methodology is applied to the methodology based on the pressure differences (eq. 11), with the distinction that we apply the smoothing and noise estimation procedures only on the resulting pressure differences.

Results

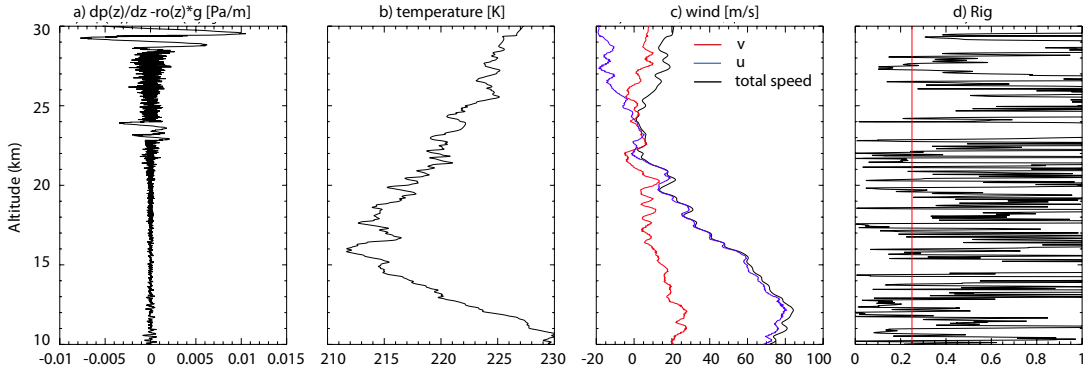

Figure 1. Vertical profiles retrieved from high vertical-resolution radiosonde data at Tateno station (36.06 °N, 140.13 °E), Japan, on 2009/21/12 (11:30 local time): (a) HBD method with subtracted background [10-point (50 m) running mean], (b) integral HBD method with subtracted background [10-point (50 m) running mean], c) horizontal wind speed (u: blue, v: red) and (d) gradient Richardson number (instability threshold

0.25 is highlighted by a red curve). The dashed line in each plot represents the tropopause height. Note that only data at 10 km and higher are shown.

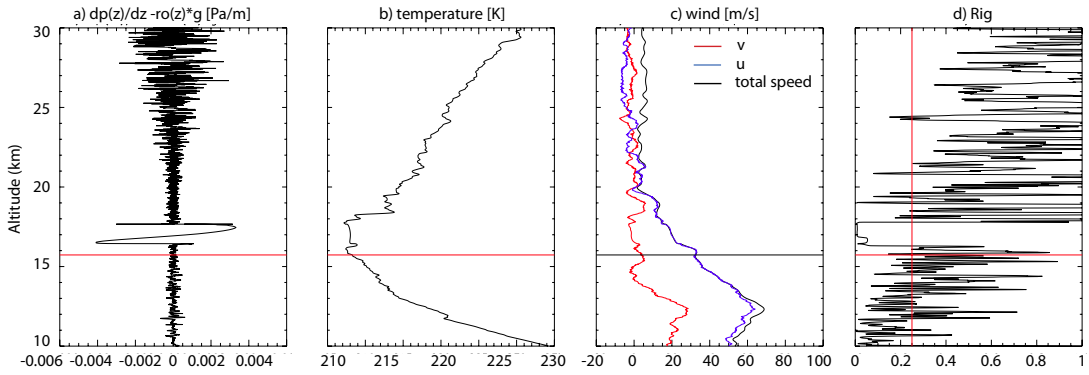

Figure 2. Vertical profiles retrieved from high vertical-resolution radiosonde data at Tateno station (36.06 °N, 140.13 °E), Japan, on 2011/06/05 (11:30 local time): (a) HBD method with subtracted background [10-point (50 m) running mean], (b) temperature, c) horizontal wind speed (u: blue, v: red) and (d) gradient Richardson number (instability threshold 0.25 is highlighted by a red curve). The solid red horizontal line in each plot represents the tropopause height. Note that only data at 10 km and higher are shown.

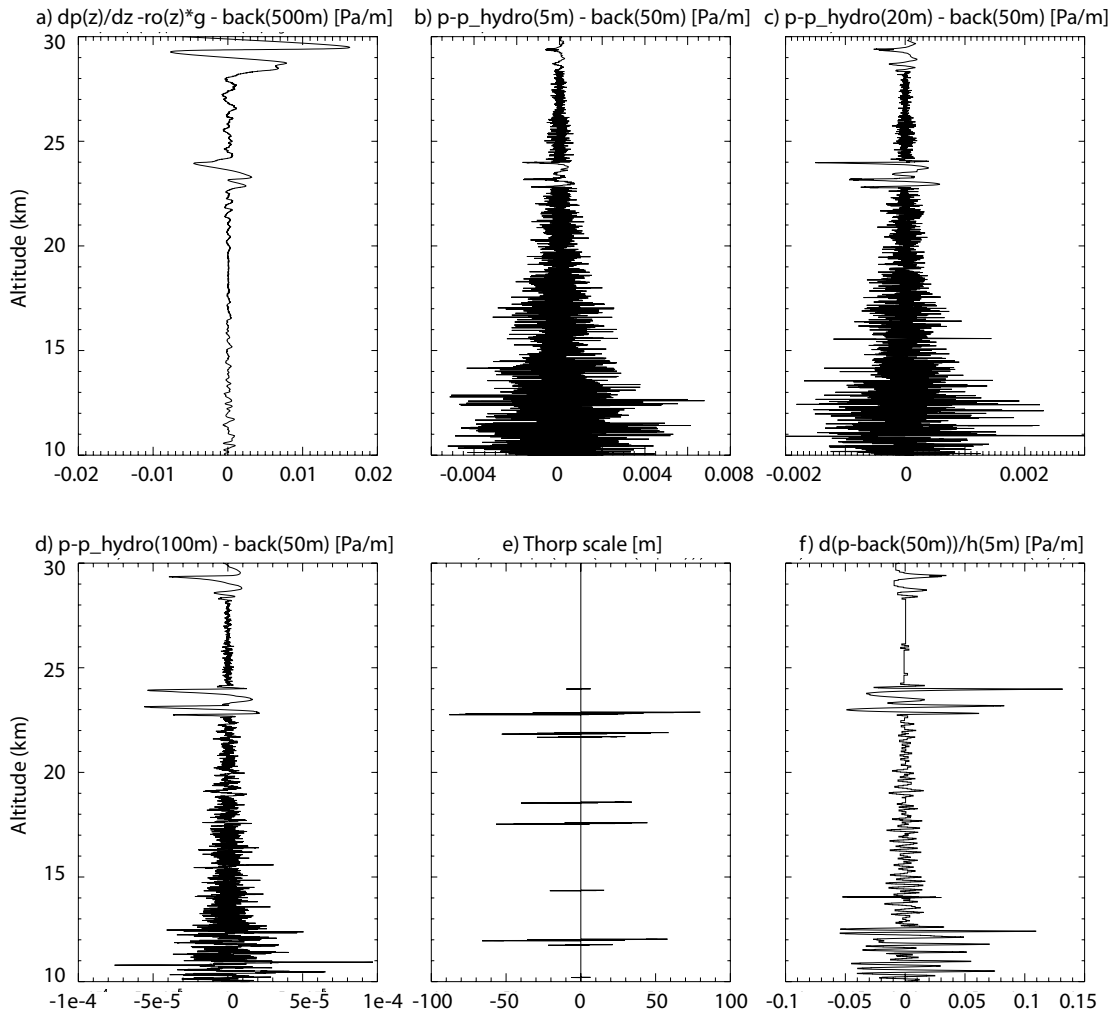

Figure 3. Vertical profiles retrieved from high vertical-resolution radiosonde data at Tateno station (36.06 °N, 140.13 °E), Japan, on 2009/21/12 (11:30 local time): (a) HBD method with subtracted background [100-point (500 m) running mean], (b) integral HBD method with $h = 5$ m and subtracted background [10-point (50 m) running mean], (c) integral HBD method with $h = 20$ m and subtracted background [10-point (50 m) running mean], (d) integral HBD method with $h = 100$ m and subtracted background [10-point (50 m) running mean], (e) Thorpe displacements after the noise reducing procedure and (f) pressure perturbation differences between the adjacent layers after background subtraction [10-point (50 m) running mean] and after the noise reducing procedure.

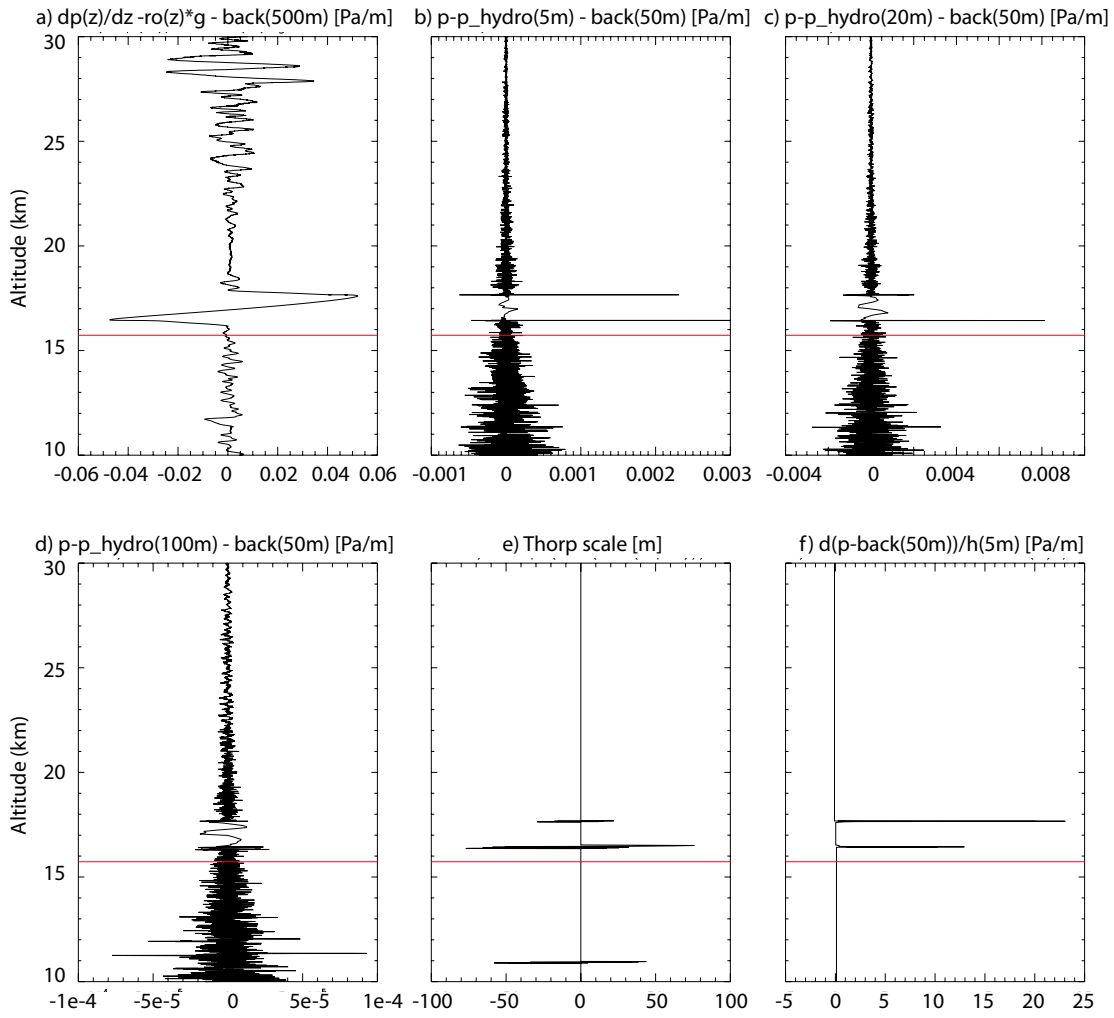

Figure 4. Vertical profiles retrieved from high vertical-resolution radiosonde data at Tateno station (36.06 °N, 140.13 °E), Japan, on 2011/06/05 (11:30 local time): (a) HBD method with subtracted background [100-point (500 m) running mean], (b) integral HBD method with $h = 5$ m and subtracted background [10-point (50 m) running mean], (c) integral HBD method with $h = 20$ m and subtracted background [10-point (50 m) running mean], (d) integral HBD method with $h = 100$ m and subtracted background [10-point (50 m) running mean], (e) Thorpe displacements after the noise reducing procedure and (f) pressure perturbation differences between the adjacent layers after background subtraction [10-point (50 m) running mean] and after the noise reducing procedure. The solid red line in each plot represents the tropopause height.

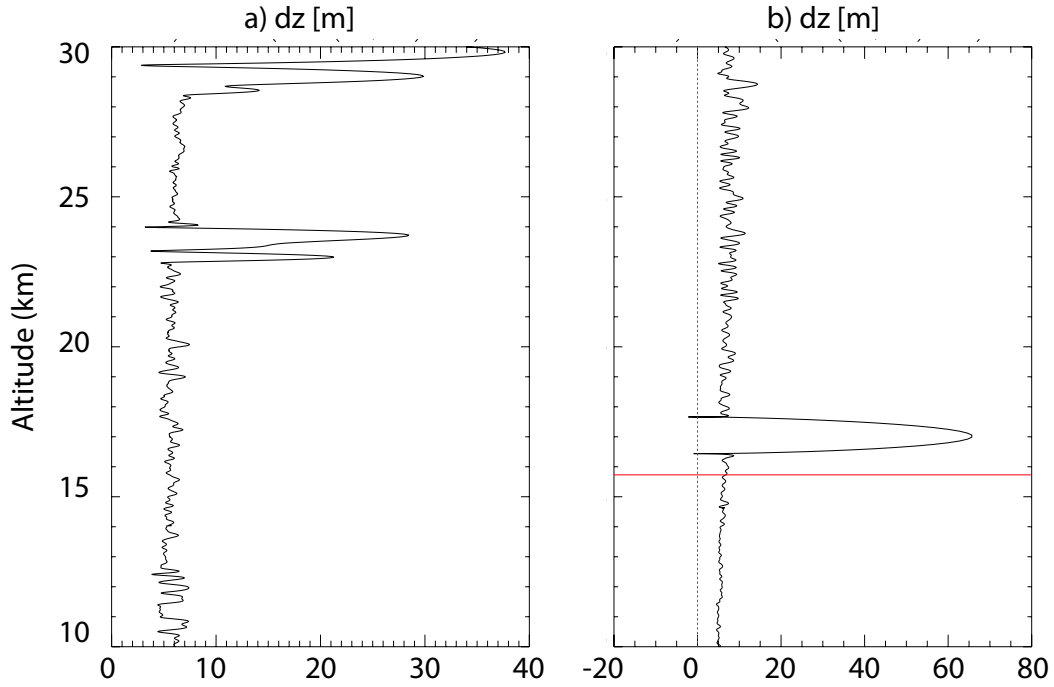

Figure 5. Vertical profiles of the vertical distance between the measurements levels for high vertical-resolution radiosonde data at Tateno station (36.06 °N, 140.13 °E), Japan: (a) on 2009/21/12 (11:30 local time) and (b) on 2011/06/05 (11:30 local time).

Discussion

In this study we presented a method for identification and analysis of overturning turbulence from HVRRD that arises after some manipulation directly from the vertical component of Euler equations. The method is based on deviations from local hydrostatic balance, thereafter its acronym - the HBD method. After deriving integral version of HBD, based on an ideal overturn, we discussed the typical pattern that is anticipated in the HBD profile in a case of the turbulence detection. We demonstrate the methodology on two illustrative observational events and show the utility of the HBD method by comparing the results with traditional diagnostics. HBD detects the turbulence, where it is to be expected based on the meteorological conditions and, in comparison with the classical Thorpe analysis, HBD detects less turbulent layers but with a greater spatial scale of the overturns.

To sum up, there is a great potential for a broad utilization of the HBD based methods for observational turbulence analyses. The issues that need to be addressed in a future work are the automatization of the method (including the choice of background or h for the best signal to noise ratio), so that it can be utilized for a global climatological study and the relation of the HBD results to turbulence characteristics (like outer and inner scale of the turbulence, energy dissipation) needs to be established. Other than that, the number of false turbulent detections using the Thorpe analysis can be immediately reduced by a supplementing information on a vertical step profile or by the easy to compute dynamic pressure analogy method (eq. 11).

Acknowledgements

The research stay of Petr Šácha at BOKU Wien is funded by the project CZ.02.2.69/0.0/0.0/19_074/0016231 International mobility of researchers at Charles University (MSCA-IF III). During the early stages of the manuscript preparation Petr Šácha was supported through a postdoctoral grant of the Xunta de Galicia ED481B 2018/103 and together with Petr Pišoft was also partly supported by GA CR under grant nos. 16-01562J and 18- 01625S. Further, Petr Sacha would like to acknowledge discussions with Harald Rieder at BOKU and at ISSI Bern with members of the New Quantitative Constraints on Orographic Gravity Wave Stress and Drag Satisfying Emerging Needs in Seasonal-to-Subseasonal and Climate Prediction.

Reference

Balsley, B.B., Kantha, L., Colgan, W., On the use of Slow Ascent Meter-Scale Sampling (SAMS) radiosondes for observing overturning events in the free atmosphere. J. Atmos. Oceanic Technol., 2010, 27, 766–775.

Birner, T., Fine-scale structure of the extratropical tropopause region. Journal of Geophysical Research, 2006, 111, D04104, https://doi.org/10.1029/2005JD006301

Caillol, P., and Zeitlin, V., Kinetic equations and stationary energy spectra of weakly nonlinear internal gravity waves. Dynamics of atmospheres and oceans, 32.2, 2000: 81-112.

Clayson, C., A., and Kantha, L., On turbulence and mixing in the free atmosphere inferred from high-resolution soundings. Journal of Atmospheric and Oceanic Technology, 2008, 25(6), 833–852. https://doi.org/10.1175/2007JTECHA992.1

Dewan, E. M., Turbulent vertical transport due to thin intermittent mixing layers in the stratosphere and other stable fluids. Science, 1981, 211(4486), 1041-1042.

Dillon, T. M., Vertical overturns: A comparison of Thorpe and Ozmidov length scales. J. Geophys. Res., 1982, 87, 9601–9613.

Dirksen, R. J., Sommer, M., Immler, F. J., Hurst, D. F., Kivi, R., and Vömel, H.: Reference quality upper-air measurements: GRUAN data processing for the Vaisala RS92 radiosonde, Atmos. Meas. Tech., 2014, 7, 4463–4490, https://doi.org/10.5194/amt-7-4463-2014.

Durre, I., Yin, X., Vose, R. S., Applequist, S., & Arnfield, J., Enhancing the data coverage in the Integrated Global Radiosonde Archive. Journal of Atmospheric and Oceanic Technology, 2018, 35(9), 1753–1770. https://doi.org/10.1175/JTECH-D-17-0223.1

Fritts, D. C., and Alexander, M. J., Gravity wave dynamics and effects in the middle atmosphere, Rev. Geophys., 2003, 41(1), 1003, doi:10.1029/2001RG000106.

Gallice, A., F. G. Wienhold, C. R. Hoyle, F. Immler, and T. Peter, Modeling the ascent of sounding balloons: Derivation of the vertical air motion. Atmos. Meas. Tech., 2011, 4, 2235–2253, doi:10.5194/amt-4-2235-2011.

Gavrilov, N.M., Luce, H., Crochet, M., Dalaudier, F., Fukao, S., Turbulence parameter estimations from high-resolution balloon temperature measurements of the MUTSI-2000 campaign. Ann. Geophys., 2005, 23, 2401–2413.

Geller, M. A., Wang, L., Chun, H.-Y., & Love, P. T., Fine-scale atmospheric processes and structures. 2017, SPARC, 49, 10–20.

Hoblit, F. M., Gust Loads on Aircraft: Concepts and Applications, 306 pp., Am. Inst. of Aeronaut. and Astronaut., Washington, D. C., 1988.

Immler, F. J., Dykema, J., Gardiner, T., Whiteman, D. N., Thorne, P. W., and Vömel, H.: Reference Quality Upper-Air Measurements: guidance for developing GRUAN data products, Atmos. Meas. Tech., 2010, 3, 1217–1231, https://doi.org/10.5194/amt-3-1217-2010, 2010.

Ingleby, B., Pauley, P., Kats, A., Ator, J., Keyser, D., Doerenbecher, A., et al., Progress toward high-resolution, real-time radiosonde reports. Bulletin of the American Meteorological Society, 2016, 97(11), 2149–2161. https://doi.org/10.1175/BAMS-D-15-00169.1

Jensen, M. P., Holdridge, D. J., Survo, P., Lehtinen, R., Baxter, S., Toto, T., and Johnson, K. L.: Comparison of Vaisala radiosondes RS41 and RS92 at the ARM Southern Great Plains site, Atmos. Meas. Tech., 2016, 9, 3115–3129, https://doi.org/10.5194/amt-9-3115-2016.

Kantha, L. and Hocking, W., Dissipation rates of turbulence kinetic energy in the free atmosphere: MST radar and radiosondes. Journal of Atmospheric and Solar-Terrestrial Physics, 2011, 73(9), 1043–1051. https://doi.org/10.1016/j.jastp.2010.11.024

Ko, H.-C., Chun, H.-Y., Wilson, R., & Geller, M. A., Characteristics of atmospheric turbulence retrieved from high vertical-resolution radiosonde data in the United States. Journal of Geophysical Research: Atmospheres, 2019, 124, 7553–7579. https://doi.org/ 10.1029/2019JD030287

Kunkel, D., Hoor, P. and Wirth, V., Can inertia-gravity waves persistently alter the tropopause inversion layer?, Geophysical Research Letters, 2014, 41(22), 7822–7829, doi: 10.1002/2014GL061970.

Osman, M. K., Hocking, W. K., & Tarasick, D. W., Parameterization of large-scale turbulent diffusion in the presence of both well- mixed and weakly mixed patchy layers. Journal of Atmospheric and Solar-Terrestrial Physics, 2016, 143-144, 14–36. https://doi.org/10.1016/j. jastp.2016.02.025.

Pisoft, P., Sacha, P., Miksovsky, J., Huszar, P., Scherllin-Pirscher, B., and Foelsche, U.: Revisiting internal gravity waves analysis using GPS RO density profiles:

comparison with temperature profiles and application for wave field stability study, Atmos. Meas. Tech., 2018, 11, 515–527, https://doi.org/10.5194/amt-11-515-2018.

Seidel, D. J., Ao, C. O., & Li, K., Estimating climatological planetary boundary layer heights from radiosonde observations: Comparison of methods and uncertainty analysis. Journal of Geophysical Research, 2010, 115, D16113. https://doi.org/10.1029/ 2009JD013680

Sharman, R. D., Trier, S. B., Lane, T. P. and Doyle, J. D., Sources and dynamics of turbulence in the upper troposphere and lower stratosphere: A review, Geophys. Res. Lett., 2012, 39, L12803, doi:10.1029/2012GL051996.

Sidi, C. and Dalaudier, F., Turbulence in the stratified atmosphere: Recent theoretical developments and experimental results, Adv. in Space Res., 10, 1990, pp. 25-36.

Smyth, W. D., and J. N. Moum, Length scales of turbulence in stably stratified mixing layers. Phys. Fluids, 2000, 12, 1327–1342.

Staquet, C., and Sommeria, J., Internal gravity waves: From instabilities to turbulence, Annu. Rev. Fluid Mech., 2002, 34, 559–593, doi:10.1146/annurev.fluid.34.090601.130953.

Sutherland, B. R.: Internal Gravity Waves, 2010, Cambridge University Press, Cambridge.

Šácha, P., Kuchař, A., Jacobi, C., and Pišoft, P.: Enhanced internal gravity wave activity and breaking over the northeastern Pacific–eastern Asian region, Atmos. Chem. Phys., 2015, 15, 13097–13112, https://doi.org/10.5194/acp-15-13097-2015.

Thorpe, S. A., Turbulence and mixing in a Scottish Loch. Philos. Trans. Roy. Soc. London, 1977, 286A, 125–181.

Tvaryanas, A. P., Epidemiology of turbulence-related injuries in air- line cabin crew, 1992–2001, Aviat. Space Environ. Med., 2003, 74, 970–976.

Vallis, Geoffrey K. Atmospheric and oceanic fluid dynamics. Cambridge University Press, 2017.

Vanneste, J., & Haynes, P. H., Intermittent mixing in strongly stratified fluids as a random walk. Journal of Fluid Mechanics, 2000, 411, 165–185. https://doi.org/10.1017/S0022112099008149

Wheelon, A. D., Weak Scattering. Vol. 2, Electromagnetic Scintillation, Cambridge University Press, 440 pp, 2003.

Wilson, R., Dalaudier, F. and Luce, H., Can one detect small-scale turbulence from standard meteorological radiosondes? Atmospheric Measurement Techniques, 2011, 4(5), 795–804. https://doi.org/10.5194/amt-4-795-2011

Wilson, R., Luce, H., Dalaudier, F. and Lefrère, J., Journal of Atmospheric and Oceanic Technology, 2010, 27(6), 977–993. https://doi.org/10.1175/2010JTECHA1357.1

Wilson, R., Luce, H., Hashiguchi, H., Shiotani, M., & Dalaudier, F., On the effect of moisture on the detection of tropospheric turbulence from in situ measurements. Atmospheric Measurement Techniques, 2013, 6(3), 697–702. https://doi.org/10.5194/amt-6-697-2013.

Wyngaard, J. C., Turbulence in the Atmosphere. Cambridge University Press, 2010.

Yoo, J.-H., Choi, T., Chun, H.-Y., Kim, Y.-H., Song, I.-S., & Song, B.-G., Inertia-gravity waves revealed in radiosonde data at Jang Bogo Station, Antarctica (74°37′S, 164°13′E). Part I: Characteristics, energy, and momentum flux. Journal of Geophysical Research: Atmospheres, 2018, 123, 13,305–13,331. https://doi.org/10.1029/2018JD029164